Optical atomic clock comparison through turbulent air

Martha I. Bodine,[1] Jean-Daniel Deschênes,[2] Isaac H. Khader,[1,3] William C. Swann,[1] Holly Leopardi,[1,3] Kyle Beloy,[1] Tobias Bothwell,[4] Samuel M. Brewer,[1] Sarah L. Bromley,[4] Jwo-Sy Chen,[1] Scott A. Diddams,[1,3] Robert J. Fasano,[1] Tara M. Fortier,[1] Youssef S. Hassan,[1,4] David B. Hume,[1] Dhruv Kedar,[4] Colin J. Kennedy,[1,4] Amanda Koepke,[1] David R. Leibrandt,[1] Andrew D. Ludlow,[1] William F. McGrew,[1] William R. Milner,[4] Daniele Nicolodi,[1,3] Eric Oelker,[1,4] Thomas E. Parker,[1] John M. Robinson,[4] Stefania Romish,[1] Stefan A. Schäffer,[1] Jeffrey A. Sherman,[1] Lindsay Sonderhouse,[4] Jian Yao,[1] Jun Ye,[1,4] Xiaogang Zhang,[1,3] Nathan R. Newbury,[1] and Laura C. Sinclair[1]

[1]*National Institute of Standards and Technology, 325 Broadway, Boulder, Colorado 80305, USA*

[2]*Octosig Consulting, Québec, Québec G1V 0A6, Canada*

[3]*Department of Physics, University of Colorado, Boulder, Colorado 80309, USA*

[4]*JILA, University of Colorado, Boulder, Colorado 80309, USA*

(Received 1 June 2020; accepted 4 August 2020; published 11 September 2020)

We use frequency-comb-based optical two-way time-frequency transfer (O-TWTFT) to measure the optical frequency ratio of state-of-the-art ytterbium and strontium optical atomic clocks separated by a 1.5-km open-air link. Our free-space measurement is compared to a simultaneous measurement acquired via a noise-cancelled fiber link. Despite nonstationary, ps-level time-of-flight variations in the free-space link, ratio measurements obtained from the two links, averaged over 30.5 hours across six days, agree to 6×10^{-19}, showing that O-TWTFT can support free-space atomic clock comparisons below the 10^{-18} level.

DOI: 10.1103/PhysRevResearch.2.033395

Optical atomic clocks, with stabilities and accuracies now approaching 10^{-18} [1–10], have created new opportunities for precision measurements in physics. These include the redefinition of the SI second, relativistic geodesy, investigation of possible variations in fundamental constants, and searches for dark matter, among others [11–24]. These applications require comparisons between clocks, and they have motivated optical atomic clock comparisons both within the same laboratory [1–4,15–17,25–28] and over fiber-optic links between laboratories [15,16,19,20,29–31]. However, recent progress in the development of high-performance portable atomic clocks [20,32–34], as well as continued interest in links between airborne or spaceborne clocks [35–50], highlights the need for methods of comparing atomic clocks over free-space links. Ideally, such methods would have residual instabilities and inaccuracies below those of the clocks themselves, despite the inevitable presence of atmospheric turbulence and platform motion.

To this end, we have explored frequency-comb-based optical two-way time-frequency transfer (O-TWTFT) across km-scale distances through turbulent air [42–48]. In previous experiments, our two optical clocks consisted of frequency combs phase-locked to cavity-stabilized lasers, which served as optical reference oscillators. With these clocks, O-TWTFT was used to compare the optical phase of two 195-THz (1535-nm) oscillators to below 10 milliradians [42], to compare their relative frequencies to fractional instabilities below 10^{-18} [42,43], and to actively synchronize two clocks to within a femtosecond, despite turbulence-induced signal fades and Doppler shifts due to motion [43–47].

In this work, we demonstrate the advancement of O-TWTFT in several ways. First, we demonstrate the capability of O-TWTFT to compare optical atomic clocks with transition frequencies that differ by over 90 THz. Second, we operate the O-TWTFT system in a new mode, allowing direct measurement of the frequency ratio of the two clocks. Finally, we confirm that O-TWTFT does not contribute any additional noise or systematic bias; the overall ratio uncertainty is limited by the clocks themselves, despite ps-level time-of-flight fluctuations in the transmitted optical timing signals.

The frequency ratio measurements discussed in this paper were performed during a measurement campaign conducted by the Boulder Area Clock and Optical Network (BACON) collaboration [51]. This campaign compared three state-of-the-art optical atomic clocks: a ytterbium (Yb) lattice clock [4], an aluminum ion (Al^+) clock [5], and a strontium (Sr) lattice clock [7]. Here, we describe measurements of the ratio of ^{171}Yb and ^{87}Sr transition frequencies, obtained over six days using O-TWTFT across a free-space optical link. We compare these measurements with frequency ratio measurements simultaneously obtained using a conventional noise-cancelled fiber link [52,53]. Additionally, we evaluate the residual instability of the measurement network through a loopback test. We find that the frequency ratios measured by the free-space and fiber links agree to an uncertainty of 6×10^{-19}, and the instability of

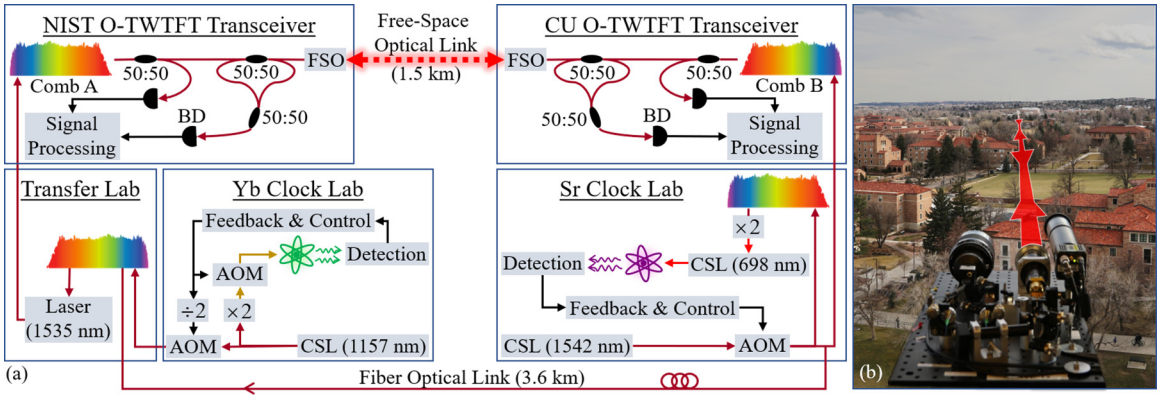

FIG. 1. (a) In the Yb Clock Lab, frequency-doubled light from a 1157-nm cavity stabilized laser (CSL) is steered into resonance with the ^{171}Yb atomic transition via frequency shifts from an acousto-optic modulator (AOM). This steered 1157-nm light is sent to the Transfer Lab, where a fiber comb [55] transfers the frequency stability and accuracy of this 1157-nm light to a 1535-nm laser. This laser light is then sent to a rooftop laboratory where it serves as the reference for comb A within the O-TWTFT transceiver. In the Sr Clock Lab, the frequency of a 698-nm CSL is steered into resonance with the ^{87}Sr atomic transition. The 698-nm light is steered by adjusting the frequency of a low-noise 1542-nm CSL [56]. A frequency comb then acts to transfer the frequency adjustments of the 1542-nm light to the 698-nm light. The steered 1542-nm light also serves as the reference for comb B within the O-TWTFT transceiver. On both sides of the free-space link, the heterodyne beat between local and remote comb pulses is detected and processed within the O-TWTFT transceivers. Additionally, the atomic clock frequencies are compared via a noise-cancelled fiber link. BD: Balanced detector. (b) Photo from O-TWTFT transceiver at CU, looking toward NIST. A free-space optical (FSO) terminal with active beam steering maintains the bidirectional link between sites (photo edited to remove window frame).

the loopback test reaches 1.5×10^{-18} at a 1000-s averaging time.

The complexity of the experimental setup (Fig. 1) reflects the fact that the ^{171}Yb and ^{87}Sr atomic transition frequencies cannot be compared directly. The atomic transitions are separated in frequency by almost 90 THz, and the clocks themselves by 1.5 km. The Yb clock is located at the National Institute of Standards and Technology (NIST), while the Sr clock is located at the University of Colorado Boulder (CU). To enable the comparison, two optical frequency synthesis chains create phase-coherent connections between the atomic transition frequencies and the frequency combs within two associated O-TWTFT transceivers.

Inside the Yb Clock Lab at NIST, frequency-doubled light from a 259.1-THz (1157-nm) cavity-stabilized laser (the Yb clock laser) is maintained on resonance with the ^{171}Yb $6s^2\ {}^1S_0 - 6s\,6p\ {}^3P_0$ transition frequency at 518.3 THz (578 nm). An optical frequency synthesis chain then connects this Yb atomic resonance frequency to the comb tooth frequencies of comb A, located within the NIST O-TWTFT transceiver [43,46]. Similarly, inside the Sr Clock Lab, the 429.2-THz (698-nm) output frequency of a cavity-stabilized laser (the Sr clock laser) is maintained on resonance with the ^{87}Sr $5s^2\ {}^1S_0 - 5s\,5p\ {}^3P_0$ transition. A second optical frequency synthesis chain connects the Sr atomic resonance frequency to the comb tooth frequencies of comb B, located within the CU O-TWTFT transceiver.

To achieve a line-of-sight link over the city of Boulder, the two O-TWTFT transceivers were placed in a rooftop laboratory at NIST and in an 11th floor conference room at CU. Two low-insertion loss, free-space optical terminals [54] enabled bidirectional transmission of comb light between the two transceivers. Before transmission, the comb light was spectrally filtered to a 1.5-THz (12-nm) bandwidth centered at 192 THz (1560 nm). Additionally, to avoid receiver saturation, comb launch powers were attenuated by 3–10 dB from an initial in-band power of 5 mW.

The mathematical description of the optical frequency syntheses provides the following, exact relationship between the atomic frequency ratio and the repetition frequency ratio of combs A and B:

$$\frac{\nu_{\mathrm{Yb}}}{\nu_{\mathrm{Sr}}} = C_1 + C_2 \frac{f_{r,A}}{f_{r,B}}. \tag{1}$$

Here, $f_{r,A}$ and $f_{r,B}$ are the repetition frequencies of combs A and B, respectively; ν_{Yb} is the ^{171}Yb transition frequency; ν_{Sr} is the ^{87}Sr transition frequency; and constants C_1 and C_2 are known quantities—linear combinations of the optical and rf frequencies in the optical frequency synthesis chains. (See Supplemental Material [57] for a derivation.) We use O-TWTFT to measure the repetition frequency ratio $f_{r,A}/f_{r,B}$ in the optical domain, with high precision, despite time-of-flight variations from turbulence or building sway. Then, using Eq. (1), we compute the atomic frequency ratio from the measured repetition frequency ratio.

To avoid the inaccuracy associated with direct photodetection of pulse arrival times, O-TWTFT uses a linear optical sampling scheme to extract the relative frequencies of the combs [58]. The repetition frequencies of combs A and B, both near 200 MHz, are deliberately offset by $\Delta f_r = f_{r,A} - f_{r,B} \approx 2.3$ kHz. In each O-TWTFT transceiver, the pulse train of the local comb is mixed with the incoming pulse train from the remote comb. The resulting optical interference pattern is a series of interferograms, repeating at ∼2.3 kHz. In both O-TWTFT transceivers, interferograms are digitized by an analog-to-digital converter (ADC) and processed to extract the exact times at which interferogram envelope maxima occurred. We refer to these extracted times as time stamps,

denoting them k_A and k_B in the NIST and CU transceivers, respectively.

For precise frequency ratio measurements, avoiding the introduction of an external, cesium-based timescale is critical. Consequently, in both transceivers, the ADCs are clocked off the local comb's repetition frequency. One increment of ADC clock time k is equal to the spacing between local comb pulses, and time stamps have units of local ADC clock cycles, rather than seconds. Following [41,43,46], we label successive interferogram maxima with integer indices p and write the time stamps as

$$k_A[p] = \frac{f_{r,A}}{\Delta f_r} p - \frac{f_{r,A} f_{r,B}}{\Delta f_r} T_{\text{link}}[p] \tag{2}$$

and

$$k_B[p] = \frac{f_{r,B}}{\Delta f_r} p + \frac{f_{r,A} f_{r,B}}{\Delta f_r} T_{\text{link}}[p], \tag{3}$$

where T_{link} is the varying time-of-flight across the reciprocal free-space path. Note that interferogram maxima are fitted with subcycle accuracy, localized to 1/1024th of an ADC clock cycle (roughly 5 ps). Consequently, time stamps k_A and k_B are noninteger. Although the time stamps have units of ADC clock cycles, considering their approximate value in seconds can be helpful. If, for example, one divides each side of Eq. (2) by the local ADC clock rate, $f_{r,A}$, then the time stamps are scaled to nominal units of seconds, with an approximate spacing $\Delta f_r^{-1} \approx 435\ \mu$s.

Were it not for ps-level, nonstationary variations in T_{link}, the combs' repetition frequency ratio could be obtained from a single set of time stamps, i.e., from either Eq. (2) or Eq. (3). Fortunately, the effects of time-of-flight variation may be eliminated by summing Eqs. (2) and (3), giving

$$k_{\text{sum}}[p] = \frac{f_{r,A} + f_{r,B}}{f_{r,A} - f_{r,B}} p, \tag{4}$$

as illustrated in Fig. 2. The slope of k_{sum} vs p, obtained using ordinary least squares (OLS) fitting, is rearranged to find the comb repetition frequency ratio $f_{r,A}/f_{r,B}$ and then, using Eq. (1), the atomic frequency ratio. Equation (4) is very sensitive to changes in the repetition frequency. Consider a small fractional frequency change $(\delta f_{r,A}/f_{r,A})$ at the NIST site. With some manipulation, one finds the resulting fractional change in k_{sum} is greatly magnified and is given by $(\delta k_{\text{sum}}/k_{\text{sum}}) \approx M(\delta f_{r,A}/f_{r,A})$, where $M = f_{r,A}/\Delta f_r \sim 10^5$. This magnification, which arises from the linear optical sampling technique [41,43,46], underlies the precision of O-TWTFT in determining the ratio.

O-TWTFT is inherently phase-continuous because it relies on a stable, uninterrupted local timescale (as defined by pulses of the local comb) to accurately record the time stamps. Here, the local timescales are extremely stable, since they are ultimately defined by atomic transitions. They are continuous as long as the optical frequency synthesis chains maintain the phase relationships between each clock laser and comb A or B. Note that phase continuity is not broken by signal fades due to turbulence or airborne debris. Signal fades along the free-space link can only reduce the total number of recorded time stamps; they cannot affect the stability or continuity of the local timescale [42]. However, both clock downtimes (i.e., times during which clock operation falls outside normal operating conditions) and phase slips in the optical frequency synthesis chains do interrupt the local timescale. Consequently, time stamps assigned before and after such an interruption have no relationship to one another, meaning that the slope of k_{sum} in Eq. (4) may only be obtained from phase-continuous sections of data.

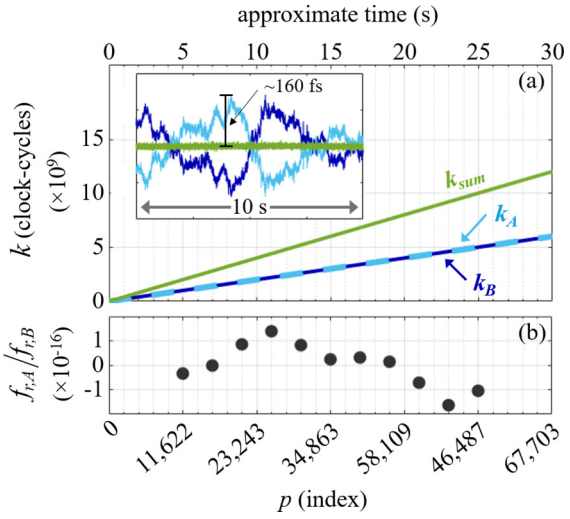

FIG. 2. (a) Time stamps k_A recorded at NIST and time stamps k_B recorded at CU, as well as their sum k_{sum}. Inset: Expanded 10-s data segment with linear fits removed. Fluctuations in k_A and k_B are caused by atmospheric turbulence and building sway. When scaled from ADC clock cycles to approximate time (scale bar), these can easily reach 100 fs in 1 s, but they are cancelled in k_{sum}. (b) Ratios of comb A and comb B repetition frequencies, offset from their mean. Each point is extracted from the slope fit to a single 10-s segment of k_{sum}.

Identifying phase-continuous data involves two steps. First, clock downtimes, logged in the Sr and Yb clock labs, are flagged as discontinuities. Second, phase slips in the optical frequency syntheses are detected by scaling k_{sum} to its approximate value in seconds and convolving it with a cycle-slip detection filter (see Supplemental Material [57]). Any sample-to-sample timing jumps greater than 1.9 fs are flagged, as 1.9 fs corresponds to a single 2π phase slip of the 578-nm Yb clock laser. Because the Yb clock laser has the highest frequency in the entire measurement system, this threshold is low enough to capture a phase slip anywhere within the optical frequency synthesis chains. The 30.5 hr of data collected during the measurement campaign contained 1201 segments of phase-continuous data, having mean, minimum, and maximum durations of 98 s, 0.01 s, and 46 min, respectively.

Within any segment of phase-continuous data, an unbiased, minimum-variance estimate of the slope of k_{sum} depends on noise statistics. In the presence of white phase noise—i.e., uncorrelated noise between summed timestamps—this estimate is obtained by OLS fitting. In the presence of white frequency noise—i.e., uncorrelated noise between successive values of the numerical derivative $k_{\text{sum}}[p] - k_{\text{sum}}[p-1]$—the mean of the derivative is the unbiased minimum-variance estimate.

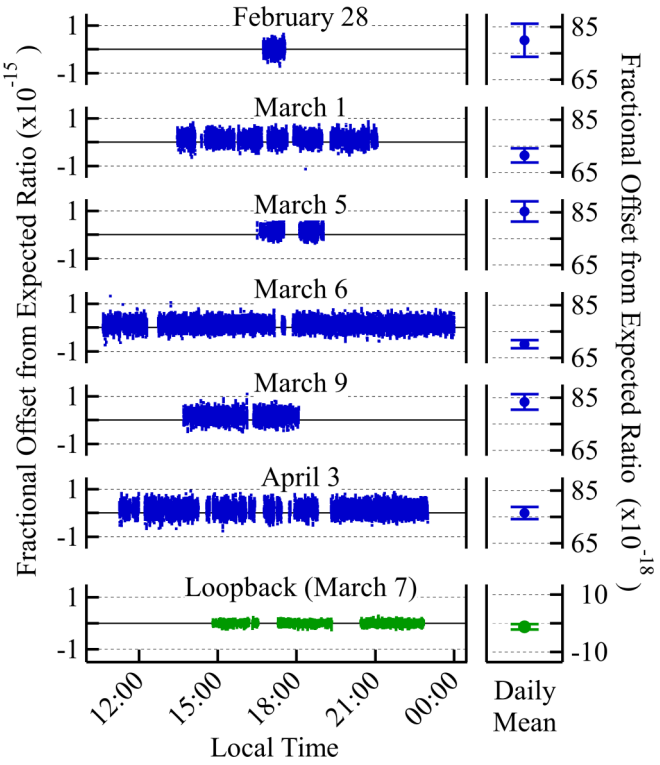

FIG. 3. Measured atomic clock frequency ratios as a function of the local time in Boulder, Colorado. Ratios are plotted as fractional offsets: (measured − expected)/(expected). The fractional offset from the expected value for the atomic frequency ratio R_{BIPM} appears significantly displaced from zero but is well within the $\pm 6.4 \times 10^{-16}$ uncertainty of R_{BIPM}. The expected value of the loopback test is 1, since this test compares the frequency of the 1542-nm CSL to itself. Uncertainty bars show 1-σ statistical uncertainty.

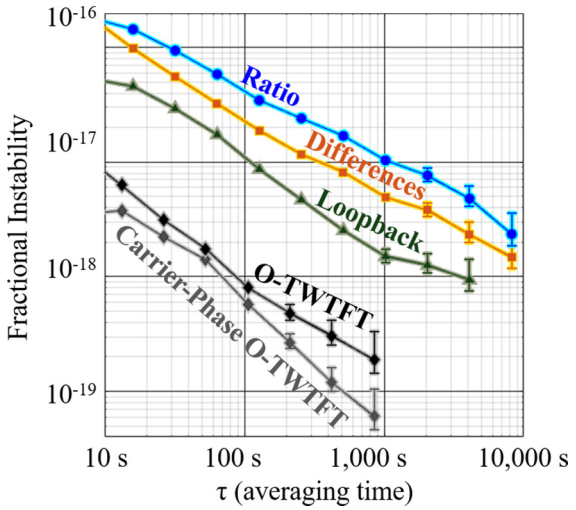

FIG. 4. Fractional instabilities (overlapping Allan deviations) of atomic frequency ratio measurements from March 6, of the differences between O-TWTFT and fiber link measurements from March 6, and of the network loopback test. Also shown is the previously measured fractional instability (modified Allan deviation) of O-TWTFT itself, as well as that of carrier-phase O-TWTFT [42].

Additionally, because both noise types are zero mean, these two estimators are unbiased for either noise type. In our data, white phase noise dominates at averaging times below 1 s (see Fig. S2) and white frequency noise (from the atom-steered clock lasers) at averaging times above 10 s. Between 1-s and 10-s averaging times, the noise is mixed. We use OLS to determine the slopes of 10-s sections within phase-continuous segments of data. (This requires rejecting segments which are phase-continuous for less than 10 s—less than 1% of the data.) These 10-s fits are overlapped by 80%, producing the frequency ratio results at 2-s intervals, as shown in Fig. 2(b). The variance penalty incurred from using this estimation method, rather than the optimal method, is below 10%. (See Supplemental Material [57] for an expanded discussion.)

Between February and April of 2018, the atomic frequency ratio was measured on six days, producing 30.5 total hours of data. Individual ratio measurements are shown in Fig. 3, as fractional offsets from the ratio R_{BIPM} calculated from the International Bureau of Weights and Measures (BIPM) values of 518 295 836 590 863.6 Hz and 429 228 004 229 873.0 Hz for Yb and Sr, respectively [59].

The overlapping Allan deviation for the ratio measurements from March 6 is shown in Fig. 4. The Allan deviation follows $3.8 \times 10^{-16}\tau^{-1/2}$, where τ is the averaging time in seconds, in accordance with the expected white frequency noise contribution from the clock lasers [51]. In other words, there is no evidence of additional noise due to the optical frequency synthesis chains or O-TWTFT. The statistical uncertainty of each daily mean in Fig. 3 is computed by extrapolating the measured Allan deviation to the full data set duration. (Systematic uncertainties are discussed in [51].)

To determine an upper limit for any residual noise from the comparison network, we perform two additional analyses. First, we carried out a network loopback test, in which the origin of both optical frequency synthesis chains was the 1542-nm CSL in the Sr Clock Lab [Fig. 1(a)]. The chain leading to the O-TWTFT transceiver at CU was unchanged, but the one at NIST was expanded to include the noise-cancelled fiber link between CU and NIST. This loopback test uses the measurement network to compare the frequency of the 1542-nm CSL to itself, thereby evaluating the cumulative statistical and systematic uncertainty of O-TWTFT, the phase-locked loops within the optical frequency synthesis chains, the noise-cancelled fiber links between laboratories, and the short, uncontrolled free-space or fiber paths within laboratories (other than those within the Yb Clock Lab). The mean of the 6-hr loopback test is offset from its expected value of 1 by $1.2 \times 10^{-18} \pm 0.9 \times 10^{-18}$, with the 1-$\sigma$ statistical uncertainty of 0.9×10^{-18} taken from the last value of the Allan deviation (Fig. 4).

Second, we compare $\nu_{\mathrm{Yb}}/\nu_{\mathrm{Sr}}$ ratio measurements obtained using O-TWTFT with simultaneous measurements obtained across a noise-cancelled fiber link [52,53]. We calculate the point-by-point differences between the O-TWTFT and fiber-link values at common measurement times, thereby removing common-mode Yb and Sr clock noise. This comparison assesses possible measurement errors between O-TWTFT and the noise-cancelled fiber link. Results, shown in Fig. 5, indicate no such errors, as the daily means of the differences are

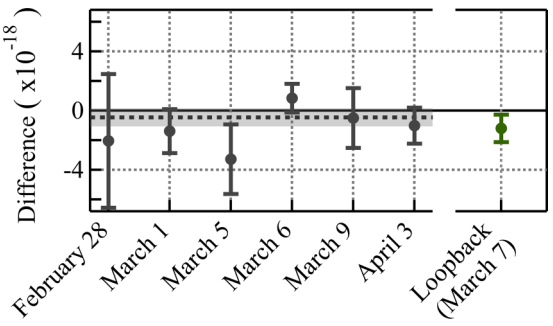

FIG. 5. Differences between O-TWTFT and fiber measurements, along with their 1-σ statistical uncertainties (error bars), their weighted average (dashed line), and its uncertainty (gray shading). Also shown is the offset of the network loopback test from its expected value of 1.

consistent with zero. Their weighted mean is $-4.5 \times 10^{-19} \pm 6 \times 10^{-19}$, well below the clocks' systematic uncertainties.

Also consistent with the removal of the common-mode clock noise, the instability of the differences is reduced compared to the instability of the ratio measurements themselves, although only by a factor of two (Fig. 4). This imperfect clock noise cancellation occurs because the two measurement approaches weight the raw data differently. The fiber link measurement uses a commercial lambda-type frequency counter, while the free-space analysis applies an overlapping parabolic filter to the raw frequency data. If the overlapping Allan deviation of the differences (Fig. 4) is extrapolated to the full 30.5-hr duration of the measurement campaign, the instability is 6×10^{-19}, consistent with the uncertainty quote above.

In conclusion, the frequency-comb-based O-TWTFT measurements reported here agree to within 6×10^{-19} with those recorded across a fiber noise-cancelled link, indicating that O-TWTFT can continue to support clock comparisons, even as clock accuracies cross below 1×10^{-18}. As transportable optical atomic clocks are developed [20,32–34], O-TWTFT will be able to support their comparisons for applications such as fundamental time metrology, relativistic geodesy measurements, or dark matter searches. With parallel work expanding the operation of O-TWTFT to longer links [45,60] and moving platforms [46,47], these comparisons could be made not only between mobile terrestrial clocks, but between future optical airborne and satellite-borne clocks as well.

We thank Frank Quinlan and Ian Coddington for comments and Michael Cermak for technical assistance. We acknowledge funding from the DARPA DSO PULSE program and NIST.

[1] C. W. Chou, D. B. Hume, J. C. J. Koelemeij, D. J. Wineland, and T. Rosenband, Frequency Comparison of Two High-Accuracy Al^+ Optical Clocks, Phys. Rev. Lett. **104**, 070802 (2010).

[2] I. Ushijima, M. Takamoto, M. Das, T. Ohkubo, and H. Katori, Cryogenic optical lattice clocks, Nat. Photonics **9**, 185 (2015).

[3] Y. Huang, H. Guan, P. Liu, W. Bian, L. Ma, K. Liang, T. Li, and K. Gao, Frequency Comparison of Two $^{40}Ca^+$ Optical Clocks with an Uncertainty at the 10^{-17} Level, Phys. Rev. Lett. **116**, 013001 (2016).

[4] W. F. McGrew *et al.*, Atomic clock performance enabling geodesy below the centimetre level, Nature (London) **564**, 87 (2018).

[5] S. M. Brewer, J.-S. Chen, A. M. Hankin, E. R. Clements, C. W. Chou, D. J. Wineland, D. B. Hume, and D. R. Leibrandt, $^{27}Al^+$ Quantum-Logic Clock with a Systematic Uncertainty below 10^{-18}, Phys. Rev. Lett. **123**, 033201 (2019).

[6] J. Keller, T. Burgermeister, D. Kalincev, A. Didier, A. P. Kulosa, T. Nordmann, J. Kiethe, and T. E. Mehlstäubler, Controlling systematic frequency uncertainties at the 10^{-19} level in linear Coulomb crystals, Phys. Rev. A **99**, 013405 (2019).

[7] T. Bothwell, D. Kedar, E. Oelker, J. M. Robinson, S. L. Bromley, W. L. Tew, J. Ye, and C. J. Kennedy, JILA SrI optical lattice clock with uncertainty of 2.0×10^{-18}, Metrologia **56**, 065004 (2019).

[8] T. L. Nicholson *et al.*, Systematic evaluation of an atomic clock at 2×10^{-18} total uncertainty, Nat. Commun. **6**, 6896 (2015).

[9] N. Huntemann, C. Sanner, B. Lipphardt, Chr. Tamm, and E. Peik, Single-Ion Atomic Clock with 3×10^{-18} Systematic Uncertainty, Phys. Rev. Lett. **116**, 063001 (2016).

[10] S. Origlia *et al.*, A high-performance optical lattice clock based on bosonic atoms, Phys. Rev. A **98**, 053443 (2018).

[11] V. A. Dzuba and V. V. Flambaum, Atomic optical clocks and search for variation of the fine-structure constant, Phys. Rev. A **61**, 034502 (2000).

[12] C. W. Chou, D. B. Hume, T. Rosenband, and D. J. Wineland, Optical clocks and relativity, Science **329**, 1630 (2010).

[13] N. Huntemann, B. Lipphardt, Chr. Tamm, V. Gerginov, S. Weyers, and E. Peik, Improved Limit on a Temporal Variation of m_p/m_e from Comparisons of Yb^+ and Cs Atomic Clocks, Phys. Rev. Lett. **113**, 210802 (2014).

[14] A. Derevianko and M. Pospelov, Hunting for topological dark matter with atomic clocks, Nat. Phys. **10**, 933 (2014).

[15] M. Takamoto *et al.*, Frequency ratios of Sr, Yb, and Hg based optical lattice clocks and their applications, C. R. Phys. **16**, 489 (2015).

[16] T. Takano, M. Takamoto, I. Ushijima, N. Ohmae, T. Akatsuka, A. Yamaguchi, Y. Kuroishi, H. Munekane, B. Miyahara, and H. Katori, Geopotential measurements with synchronously linked optical lattice clocks, Nat. Photonics **10**, 662 (2016).

[17] C. Sanner, N. Huntemann, R. Lange, C. Tamm, E. Peik, M. S. Safronova, and S. G. Porsev, Optical clock comparison for Lorentz symmetry testing, Nature (London) **567**, 204 (2019).

[18] J. Müller, D. Dirkx, S. M. Kopeikin, G. Lion, I. Panet, G. Petit, and P. N. A. M. Visser, High performance clocks and gravity field determination, Space Sci. Rev. **214**, 5 (2017).

[19] P. Delva *et al.*, Test of Special Relativity Using a Fiber Network of Optical Clocks, Phys. Rev. Lett. **118**, 221102 (2017).

[20] J. Grotti *et al.*, Geodesy and metrology with a transportable optical clock, Nat. Phys. **14**, 437 (2018).

[21] P. Delva, A. Hees, and P. Wolf, Clocks in space for tests of fundamental physics, Space Sci. Rev. **212**, 1385 (2017).

[22] C. Clivati *et al.*, A VLBI experiment using a remote atomic clock via a coherent fibre link, Sci. Rep. **7**, 40992 (2017).

[23] T. E. Mehlstäubler, G. Grosche, C. Lisdat, P. O. Schmidt, and H. Denker, Atomic clocks for geodesy, Rep. Prog. Phys. **81**, 064401 (2018).

[24] S. Bize, The unit of time: Present and future directions, C. R. Phys. **20**, 153 (2019).

[25] N. Nemitz, T. Ohkubo, M. Takamoto, I. Ushijima, M. Das, N. Ohmae, and H. Katori, Frequency ratio of Yb and Sr clocks with 5×10^{-17} uncertainty at 150 seconds averaging time, Nat. Photonics **10**, 258 (2016).

[26] N. Hinkley, J. A. Sherman, N. B. Phillips, M. Schioppo, N. D. Lemke, K. Beloy, M. Pizzocaro, C. W. Oates, and A. D. Ludlow, An atomic clock with 10^{-18} instability, Science **341**, 1215 (2013).

[27] R. M. Godun, P. B. R. Nisbet-Jones, J. M. Jones, S. A. King, L. A. M. Johnson, H. S. Margolis, K. Szymaniec, S. N. Lea, K. Bongs, and P. Gill, Frequency Ratio of Two Optical Clock Transitions in $^{171}Yb^{+}$ and Constraints on the Time Variation of Fundamental Constants, Phys. Rev. Lett. **113**, 210801 (2014).

[28] E. Oelker *et al.*, Optical clock intercomparison with 6×10^{-19} precision in one hour, Nat. Photonics **13**, 714 (2019).

[29] T. Rosenband *et al.*, Frequency ratio of Al^{+} and Hg^{+} single-ion optical clocks: Metrology at the 17th decimal place, Science **319**, 1808 (2008).

[30] A. Yamaguchi, M. Fujieda, M. Kumagai, H. Hachisu, S. Nagano, Y. Li, T. Ido, T. Takano, M. Takamoto, and H. Katori, Direct comparison of distant optical lattice clocks at the 10^{-16} uncertainty, Appl. Phys. Express **4**, 082203 (2011).

[31] C. Lisdat *et al.*, A clock network for geodesy and fundamental science, Nat. Commun. **7**, 12443 (2016).

[32] S. B. Koller, J. Grotti, St. Vogt, A. Al-Masoudi, S. Dörscher, S. Häfner, U. Sterr, and C. Lisdat, Transportable Optical Lattice Clock with 7×10^{-17} Uncertainty, Phys. Rev. Lett. **118**, 073601 (2017).

[33] L. Liu *et al.*, In-orbit operation of an atomic clock based on laser-cooled ^{87}Rb atoms, Nat. Commun. **9**, 1 (2018).

[34] S. Hannig, L. Pelzer, N. Scharnhorst, J. Kramer, M. Stepanova, Z. T. Xu, N. Spethmann, I. D. Leroux, T. E. Mehlstäubler, and P. O. Schmidt, Towards a transportable aluminium ion quantum logic optical clock, Rev. Sci. Instrum. **90**, 053204 (2019).

[35] K. Djerroud, O. Acef, A. Clairon, P. Lemonde, C. N. Man, E. Samain, and P. Wolf, Coherent optical link through the turbulent atmosphere, Opt. Lett. **35**, 1479 (2010).

[36] D. R. Gozzard, S. W. Schediwy, B. Stone, M. Messineo, and M. Tobar, Stabilized Free-Space Optical Frequency Transfer, Phys. Rev. Appl. **10**, 024046 (2018).

[37] M. Laas-Bourez, C. Courde, E. Samain, P. Exertier, P. Guillemot, J.-M. Torre, N. Martin, and C. Foussard, Accuracy validation of T2L2 time transfer in co-location, IEEE Trans. Ultrason. Ferroelectr. Freq. Control **62**, 255 (2015).

[38] C. Robert, J.-M. Conan, and P. Wolf, Impact of turbulence on high-precision ground-satellite frequency transfer with two-way coherent optical links, Phys. Rev. A **93**, 033860 (2016).

[39] S. Chen, F. Sun, Q. Bai, D. Chen, Q. Chen, and D. Hou, Sub-picosecond timing fluctuation suppression in laser-based atmospheric transfer of microwave signal using electronic phase compensation, Opt. Commun. **401**, 18 (2017).

[40] A. Belmonte, M. T. Taylor, L. Hollberg, and J. M. Kahn, Effect of atmospheric anisoplanatism on earth-to-satellite time transfer over laser communication links, Opt. Express **25**, 15676 (2017).

[41] F. R. Giorgetta, W. C. Swann, L. C. Sinclair, E. Baumann, I. Coddington, and N. R. Newbury, Optical two-way time and frequency transfer over free space, Nat. Photonics **7**, 434 (2013).

[42] L. C. Sinclair, H. Bergeron, W. C. Swann, E. Baumann, J.-D. Deschênes, and N. R. Newbury, Comparing Optical Oscillators across the Air to Milliradians in Phase and 10^{-17} in Frequency, Phys. Rev. Lett. **120**, 050801 (2018).

[43] J.-D. Deschênes, L. C. Sinclair, F. R. Giorgetta, W. C. Swann, E. Baumann, H. Bergeron, M. Cermak, I. Coddington, and N. R. Newbury, Synchronization of Distant Optical Clocks at the Femtosecond Level, Phy. Rev. X **6**, 021016 (2016).

[44] H. Bergeron, L. C. Sinclair, W. C. Swann, C. W. Nelson, J.-D. Deschênes, E. Baumann, F. R. Giorgetta, I. Coddington, and N. R. Newbury, Tight real-time synchronization of a microwave clock to an optical clock across a turbulent air path, Optica **3**, 441 (2016).

[45] L. C. Sinclair *et al.*, Synchronization of clocks through 12 km of strongly turbulent air over a city, Appl. Phys. Lett. **109**, 151104 (2016).

[46] L. C. Sinclair, H. Bergeron, W. C. Swann, I. Khader, K. C. Cossel, M. Cermak, N. R. Newbury, and J.-D. Deschênes, Femtosecond optical two-way time-frequency transfer in the presence of motion, Phys. Rev. A **99**, 023844 (2019).

[47] H. Bergeron, L. C. Sinclair, W. C. Swann, I. Khader, K. C. Cossel, M. Cermak, J.-D. Deschênes, and N. R. Newbury, Femtosecond time synchronization of optical clocks off of a flying quadcopter, Nat. Commun. **10**, 1819 (2019).

[48] W. C. Swann, M. I. Bodine, I. Khader, J.-D. Deschênes, E. Baumann, L. C. Sinclair, and N. R. Newbury, Measurement of the impact of turbulence anisoplanatism on precision free-space optical time transfer, Phys. Rev. A **99**, 023855 (2019).

[49] H. J. Kang, J. Yang, B. J. Chun, H. Jang, B. S. Kim, Y.-J. Kim, and S.-W. Kim, Free-space transfer of comb-rooted optical frequencies over an 18 km open-air link, Nat. Commun. **10**, 1 (2019).

[50] H. Dai *et al.*, Towards satellite-based quantum-secure time transfer, Nat. Phys. **16**, 848 (2020).

[51] Boulder Atomic Clock Optical Network (BACON) Collaboration, Frequency ratio measurements with 18-digit accuracy using a network of optical clocks, arXiv:2005.14694.

[52] S. M. Foreman, A. D. Ludlow, M. H. G. de Miranda, J. E. Stalnaker, S. A. Diddams, and J. Ye, Coherent Optical Phase Transfer over a 32-km Fiber with 1 s Instability at 10^{-17}, Phys. Rev. Lett. **99**, 153601 (2007).

[53] N. R. Newbury, P. A. Williams, and W. C. Swann, Coherent transfer of an optical carrier over 251 km, Opt. Lett. **32**, 3056 (2007).

[54] W. C. Swann, L. C. Sinclair, I. Khader, H. Bergeron, J.-D. Deschênes, and N. R. Newbury, Low-loss reciprocal optical terminals for two-way time-frequency transfer, Appl. Opt. **56**, 9406 (2017).

[55] H. Leopardi, J. Davila-Rodriguez, F. Quinlan, J. Olson, J. A. Sherman, S. A. Diddams, and T. M. Fortier, Single-branch Er:fiber frequency comb for precision optical metrology with 10^{-18} fractional instability, Optica **4**, 879 (2017).

[56] D. G. Matei *et al.*, 1.5 μm Lasers with Sub-10 mHz Linewidth, Phys. Rev. Lett. **118**, 263202 (2017).

[57] See Supplemental Material at http://link.aps.org/supplemental/10.1103/PhysRevResearch.2.033395 for Allan deviations for all six measurement days, as well as details on optical frequency synthesis chains, frequency ratio estimation, and phase-slip detection.

[58] I. Coddington, W. C. Swann, and N. R. Newbury, Coherent linear optical sampling at 15 bits of resolution, Opt. Lett. **34**, 2153 (2009).

[59] Consultative Committee for Time and Frequency, Report of the 21st Meeting to the International Committee for Weights and Measures, Bur. Int. Poids Mes., 2017.

[60] M. I. Bodine, J. L. Ellis, W. C. Swann, S. A. Stevenson, J.-D. Deschênes, E. D. Hannah, P. Manurkar, N. R. Newbury, and L. C. Sinclair, Optical time-frequency transfer across a free-space, three-node network, APL Photonics **5**, 076113 (2020).